Research Article | Vol. 30, No. 22 / 24 Oct 2022 / Optics Express 40842
Optics EXPRESS

Fabrication of ultra-high aspect ratio silicon grating using an alignment method based on a scanning beam interference lithography system

XINGSHUO CHEN,[1,2] SHAN JIANG,[1,3] YUBO LI,[1,2] YANXIU JIANG,[1] WEI WANG,[1] AND BAYANHESHIG[1,*]

[1] *Changchun Institute of Optics, Fine Mechanics and Physics, Chinese Academy of Sciences, Changchun 130033, China*
[2] *University of Chinese Academy of Sciences, Beijing 100049, China*
[3] *jiangshan0122@126.com*
[*] *bayin888@sina.com*

Abstract: The high-aspect-ratio silicon grating (HARSG) is an important X-ray optical device that is widely used in X-ray imaging and spectrum detection systems. In this paper, we propose a high-precision alignment method based on the scanning beam interference lithography (SBIL) system to realize precise alignment between the <111> orientation on the (110) wafer plane and the grating lines direction, which is an essential step in HARSG manufacture to obtain the high-aspect-ratio grating structure. After the location of the <111> orientation through fan-shaped mask etching and reference grating fabrication, a two-step method that combines static preliminary alignment and dynamic precision alignment is used to align the reference grating lines direction with the interference field fringes of the SBIL system through the interference of the diffracted light from the reference grating near the normal direction, which can realize a minimal alignment error of 0.001°. Through the overall alignment process, HARSGs with groove densities of 500 gr/mm, 1800 gr/mm, and 3600 gr/mm were fabricated through anisotropic wet etching in KOH solution, producing ultra-high aspect ratios and etch rate ratios greater than 200.

1. Introduction

Silicon-based micro-nano devices are widely used in many fields including microelectronics, micro/nano-electro-mechanical systems, and nano-optics [1–3] because of the electrical and optical properties of silicon materials. Among these devices, deeply-etched silicon gratings with ultra-high aspect ratios (high-aspect-ratio silicon gratings, or HARSGs) have attracted great attention for applications in the field of X-ray optics in recent years, such as in X-ray imaging as phase gratings and amplitude gratings [4–8], and also in X-ray energy spectrum analysis applications as efficient dispersion devices [9–11].

Compared to common grating structures, manufacturing of HARSG has been a challenge due to its extremely high aspect ratio. In previous studies, it has been demonstrated that HARSGs can be fabricated using both anisotropic wet etching [12–14] and deep reactive ion etching (DRIE) methods [9,15]. During wet etching of silicon using alkaline solutions such as KOH and tetramethylammonium hydroxide (TMAH), it is necessary to ensure alignment between the <111> orientation on the surface of the (110) silicon wafer and the direction of the grating lines to suppress transverse etching, which limits the aspect ratio of the grating structure. [14]. HARSG fabrication using DRIE is independent of the crystal orientation, but nevertheless requires a wet polishing step to reduce the high grating side wall roughness caused by the Bosch process [16], the effect of which is strongly dependent on the crystal orientation of the sidewall plane. It should be noted that metal-assisted chemical etching has also been applied to HARSG fabrication in recent years [17–20], but as a result of the edge effect and the inherent instability

#469374 https://doi.org/10.1364/OE.469374
Journal © 2022 Received 5 Jul 2022; revised 11 Aug 2022; accepted 11 Aug 2022; published 20 Oct 2022

Optics EXPRESS

of metal-assisted chemical etching, the groove density of the large-area silicon gratings obtained by this method remains limited to date. Therefore, alignment processing is an essential step in HARSG fabrication that strongly affects both the maximum aspect ratio of the grating and the grating side wall roughness.

The <111> crystal orientation of the silicon substrate must be located initially before the alignment process can be performed. A fan-shaped mask etching method [14,16,21] has been used widely during this step to locate the <111> orientation on the (110) silicon wafer, and this method can eventually locate a spoke structure that lies closest to <111> orientation. To perform alignment between the selected spoke and the grating lines, Ahn et al. [13,21] proposed a method based on the scanning beam interference lithography (SBIL) system using a microscope located above the wafer that produced an alignment error of less than 0.05°. Using the relative movement between the wafer and the microscope, the spoke direction can be adjusted gradually to match the movement direction of the wafer, which is in the same direction as the grating fringes obtained after lithography. However, this requires integration of microscopic systems into the SBIL system, which will increase the system complexity and result in long adjustment times. Zheng et al. [14] later presented an effective alignment method for a static holographic exposure system based on moiré fringes between the grating and the interference fringes; however, their method includes use of a SiO_2 reference wafer in an intermediate step, which adds to the process complexity and introduces additional errors. Additionally, the He-Ne laser used in the intermediate step determined that this method cannot be used for gratings with periods smaller than 316.4 nm. Bruccoleri et al. [16] proposed a simpler alignment method for the Mach-Zehnder holographic exposure system based on a reference grating on the wafer, and the orientation of the wafer was adjusted by overlapping the spots of diffraction light beams. However, the interference between diffracted light beams was not reported in their method, which led to a lack of accuracy in the alignment process and resulted in a large alignment error of 0.1°.

In this paper, we propose a new method for alignment between the interference fringes and the <111> orientation of the silicon wafer based on the SBIL system that consists of two main steps: i) a (110) silicon wafer with a fan-shaped mask is etched in a KOH solution to locate its <111> orientation, and a reference grating pattern is subsequently aligned with the <111> orientation and transferred onto the wafer via ultraviolet (UV) contact lithography; and ii) the interference fringes of SBIL system are aligned with the reference grating through a process of interference of the diffracted light from the reference grating; this process can be divided into static and dynamic processes to achieve ultra-high precision. The grating pattern is then exposed and transferred into the silicon nitride layer for the subsequent wet etching process. As a result, HARSGs with groove densities of 500 gr/mm, 1800 gr/mm, and 3600 gr/mm are fabricated through anisotropic wet etching in a KOH solution, demonstrating ultra-high aspect ratios and etch rate ratios.

2. Alignment method

The purpose of the alignment process is to align the interference fringe of the interference field exposure system precisely with the <111> crystal orientation on the (110) silicon wafer surface, thus enabling an ultra-high etching rate ratio to be obtained during the wet etching process. The alignment process can be divided into two main parts, as shown in Fig. 1: i) Location of the crystal orientation and fabrication of the reference grating; and ii) alignment of the reference grating with the interference fringes of the exposure system. A SBIL system in our laboratory [22–24] was used to perform the alignment and lithography processes during our experiments. The alignment process will be described in detail in this section, with particular emphasis on the alignment method between the reference grating and the interference fringes based on the SBIL system.

Optics EXPRESS

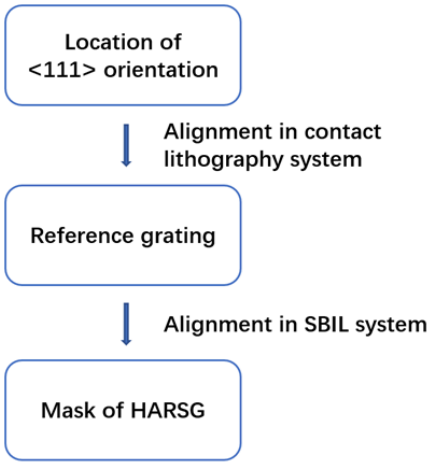

Fig. 1. Flow diagram for alignment between the <111> orientation and the direction of the grating lines.

2.1. Location of the <111> plane direction and alignment of the reference grating

In this work, the <111> orientation of the silicon wafer was located via anisotropic wet etching of a fan-shaped grating silicon nitride mask. A fan-shaped pattern with angular intervals of 0.03° was exposed on the silicon nitride surface of the wafer via UV contact lithography and was transferred into the 40-nm-thick silicon nitride layer as a wet etching mask. This wafer was then etched in a 25wt% solution at room temperature for approximately 72 hours. Because of the anisotropy of silicon when etched in an alkaline solution, the spokes near the <111> orientation had a smaller lateral etching rate and thus could be retained during the wet etching process. The etched and unetched areas of each spoke could be distinguished clearly under an optical microscope; therefore, by measuring the laterally etched width of each spoke, the spoke with the lowest undercutting could be located, which lies closest to the <111> crystal orientation. The difference in undercutting between the left and right sides of the spoke could also aid with accurate location, and the location error for this step could be considered to be half of the angular interval of the fan-shaped mask [14], which was found to be 0.015° in our experiment. Subsequently, a reference grating oriented parallel to the spoke in the <111> orientation was formed by UV contact lithography, as shown in Fig. 2. The contact mask for the reference grating contained a slit to enable alignment with the spoke in the <111> orientation by using a precision turntable and a microscope included in the contact lithography system. It is clear that the maximum alignment error is determined by the shape parameters of both the spokes and the slit, which are shown in Fig. 2(b), and this corresponds to a maximum error of 0.035°. The error can be reduced further by adjusting the lengths of the spokes and the shape of the slit, but the existing error is sufficient for fabrication of the HARSGs in our experiments. The reference grating pattern was eventually transferred into the silicon nitride layer by inductively coupled plasma (ICP) etching. For further alignment processing, the period of the reference grating must be an even multiple of the period of the interference field in the exposure system, which will be described in detail in Section 2.2.

2.2. Alignment between interference fringes and reference grating

Alignment between the interference field fringes and the reference grating was achieved via interference of the diffracted light from the reference grating through the SBIL system. Fig. 3 presents a schematic of the static alignment process. Since the reference grating period was set

Optics EXPRESS

to be an even multiple of the interference field period, two coincident diffraction beams will be generated in the normal direction of the reference grating surface in the ideal case where the two coherent beams from the exposure system both lie within the principal grating plane. In common cases in which there is a deviation between the reference grating grid line direction and the interference field direction, the left and right beams both undergo cone diffraction on the reference grating, causing these two diffracted beams to deviate from the normal direction, and resulting in formation of interference fringes within the coherent region of the diffracted beams on the detector.In addition, as shown in Fig. 3(a), diffracted light of other orders that is not oriented in the normal direction will also produce interference fringes, but nevertheless, the interference fringes produced by $\pm m$ order diffracted light beams clearly provide the best contrast because of the differences in the diffraction efficiencies of the different orders. Fig. 3(b) shows a representation of the wave vector component of the diffracted light in the O-XY plane. When an included angle α is generated between the interference fringe and the reference grating direction, the wave vector components of the $\pm m$ order diffraction light in the O-XY plane can be expressed as:

$$\boldsymbol{k}_{Dxy} = \boldsymbol{k}_{0xy} \pm m\boldsymbol{k}_g \tag{1}$$

where $\boldsymbol{k}_{0xy}$ and $\boldsymbol{k}_{Dxy}$ respectively represent the wave vector components of the incident and diffracted light in the O-XY plane, $\boldsymbol{k}_g$ is the grating vector of the reference grating, and m represents the order of the diffracted light near the normal direction, and satisfies the relationship $k_{0xy} = mk_g$. Therefore, the magnitude of $\boldsymbol{k}_{Dxy}$ can be expressed as:

$$k_{Dxy} = 2mk_g \sin\frac{\alpha}{2} \tag{2}$$

Fig. 3(b) clearly shows that the azimuth angle of the diffracted light is $1 - \alpha/2$, while the diffraction angle satisfies the following equation:

$$\sin\theta = \frac{\mathrm{k_{Dxy}}}{\mathrm{k_0}} = \frac{2\mathrm{m}\lambda\sin\frac{\alpha}{2}}{\Lambda} \tag{3}$$

where λ is the exposure wavelength and Λ represents the period of the reference grating.The angle between the two diffraction light beams is 2θ and is symmetrical with respect to the normal; the period of the interference fringes produced by two diffraction light beams can thus be obtained:

$$t = \frac{\Lambda}{4m\sin\frac{\alpha}{2}} \tag{4}$$

According to the period of double-beam interference of the exposure field in the SBIL system and the grating equation of the reference grating, it can be concluded that for normal diffraction lights of order $\pm m$, the period of the reference grating and the period of the interference field t_0 satisfy the relationship $\Lambda = 2mt_0$.Therefore, Eq. (4) can be rewritten as:

$$t = \frac{t_0}{2\sin\frac{\alpha}{2}} \tag{5}$$

Eq. (5) above can also be obtained by calculating the moiré fringe generated by two groups of interference fringes of the exposure field, and it can be seen that the period of the interference fringes produced by the diffracted light is independent of Λ and inversely proportional to α. In our experiment, a precision turntable was used in the SBIL system for fine adjustment of the wafer orientation to maximize the interference fringe period. During the alignment process, the wafer with the reference grating was initially coated with a photoresist layer and was then

Optics EXPRESS

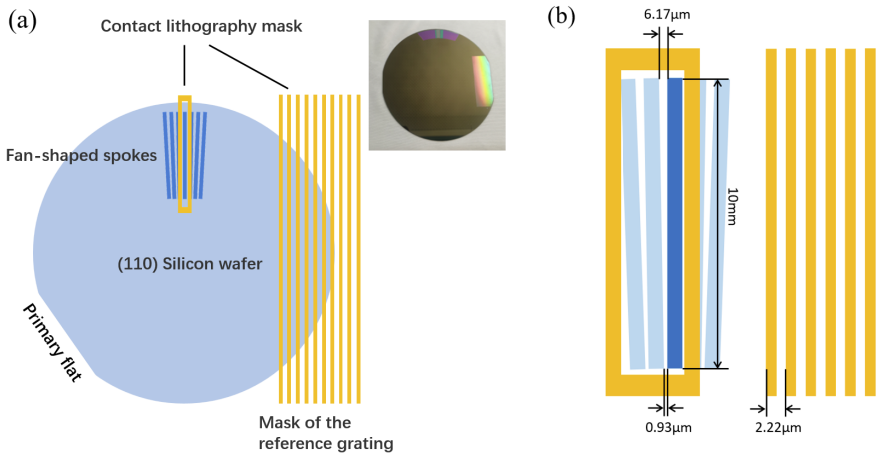

Fig. 2. (a) Diagram of the method for alignment between the contact lithography mask and the spoke in the <111> orientation. (b) Shape parameters of the contact mask and the fan-shaped spokes. Alignment is based on the edge of the slit and the edge of the selected spoke (dark blue), with accuracy that is determined by the gap between the spokes and the spoke length. The groove density of the reference grating was set to 450 gr/mm in our experiment for HARSG fabrication.

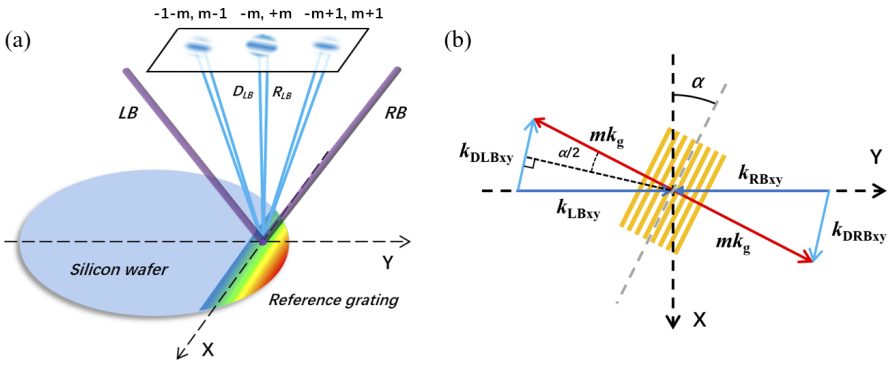

Fig. 3. Schematic diagram of alignment method based on the reference grating and the SBIL system. (b) Matching relationship between the grating vector of the reference grating and the O-XY plane component of the wave vector of the incident light beams and the $\pm m$ order diffraction lights.

placed on the turntable. As illustrated in Fig. 4, the interference field from the SBIL system was incident on the reference grating area of the wafer, and the diffracted light beams from the two exposure beams were received by the nearby detector through a mirror located above the wafer. The alignment operation was subsequently performed by adjusting the turntable to obtain a large fringe period, and the exposure process would be performed directly after the alignment via the relative movement between the interference field and the wafer. For the HARSG manufacturing experiments, the light source for the SBIL system was a laser with an operating wavelength of 413 nm, and the included angles for the two exposure beams were 22.8° and 50.9°, corresponding to the 1800 gr/mm and 3600 gr/mm interference fringes, respectively. Therefore, the groove density of the reference grating was set at 450 gr/mm, and the values of the diffraction order m near the normal direction corresponding to the groove densities of 1800 gr/mm and 3600

Optics EXPRESS

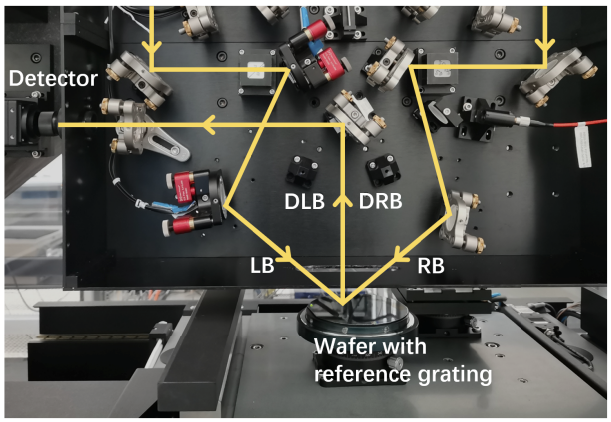

Fig. 4. Image of the alignment process between the reference grating and interference field fringes in the SBIL system.

gr/mm were 2 and 4, respectively. It should be noted that, unlike conventional holographic lithography, the size of interference field in our SBIL system was approximately 0.9 mm, and thus the period of the interference fringe from the diffraction light that could be observed directly was limited to approximately 1.8 mm, leading to alignment errors of 0.018° for the 1800 gr/mm density and 0.009° for the 3600 gr/mm density. Our etching experiment to fabricate HARSGs has already demonstrated perfect repeatability with this level of precision, but the alignment process accuracy can be improved further via a dynamic method that involves introduction of an additional phase change that results from the wafer movement within the SBIL system when the fringe period is greater than the spot size on the receiving plane. Fig. 5 illustrates the principle of the dynamic alignment process. The X-axis and Y-axis respectively represent the scanning direction and the stepping direction of the worktable in the SBIL system, and when the wafer moves by d_x in the scanning direction, this results in a relative movement by a distance d_g in the grating vector direction between the reference grating and the exposed light field, which satisfies

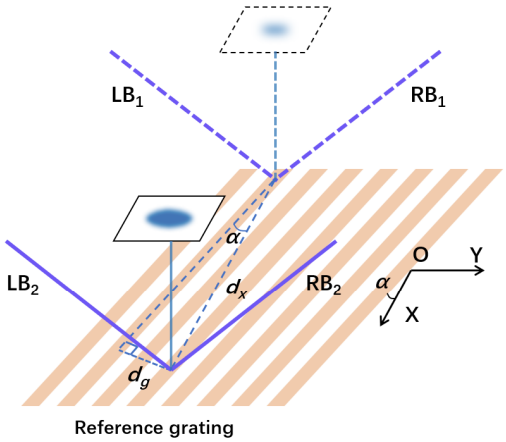

Fig. 5. Schematic diagram of the dynamic alignment process through the relative movement in x-direction between the reference grating and the exposure field. Movement perpendicular to the grating line will resulting in the phase difference between the two diffracted beams, leading to the periodic change of light intensity on the receiving plane.

Optics EXPRESS

the relation $d_g = d_x \sin\alpha$. According to grating phase shift theory, a phase difference ϕ which is related linearly to d_x will be generated between the two diffracted beams, where:

$$\phi = \frac{4m\pi d_x \sin\alpha}{\Lambda} = \frac{2\pi d_x \sin\alpha}{t_0} \tag{6}$$

Therefore, during movement of the wafer, continuous fringe movement will be observed on the receiving plane as a result of the linear phase shift, the speed of which is proportional to $\sin\alpha$.

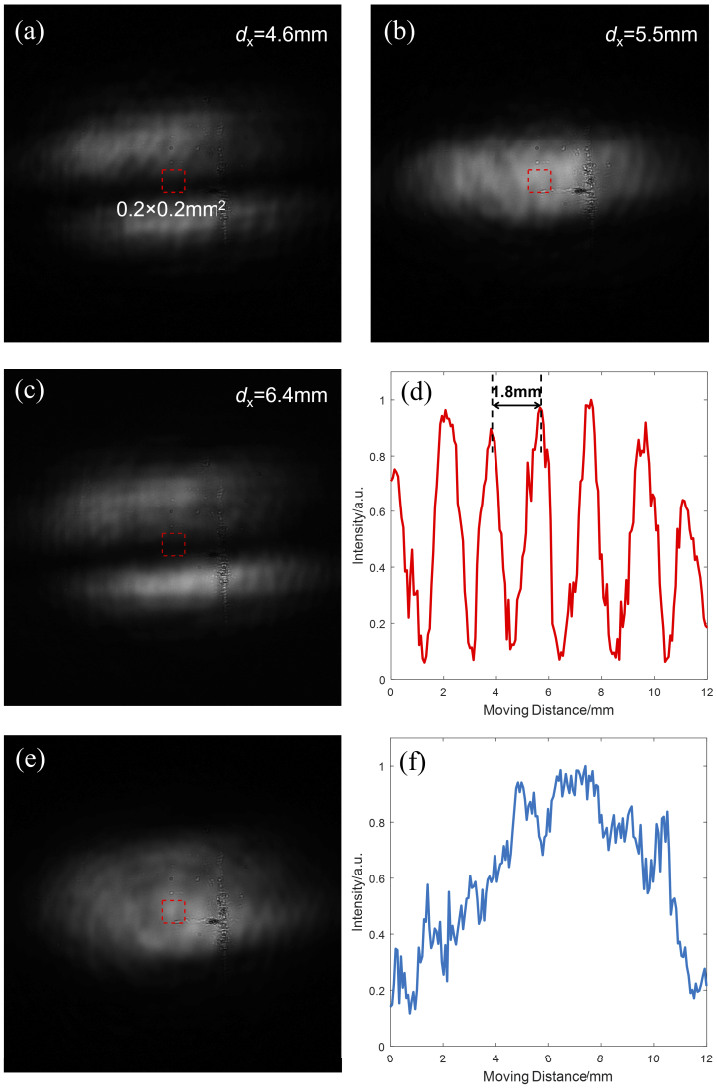

Fig. 6. Interference images of the diffracted light when the movement distance of the reference grating was (a) 4.6 mm, (b) 5.5 mm, and (c) 6.4 mm during the dynamic alignment process, providing a clear illustration of the movement of the fringes. (d) Average intensity of the red framed line area during movement of the reference grating from 0 to 12 mm, with a change period of approximately 1.8 mm. (e) and (f) show the static image and the variation in the intensity after slight adjustment of the turntable, respectively, with a much larger period of approximately 12 mm corresponding to a deviation angle of 0.001°.

Optics EXPRESS

Fig. 6 shows an example of this method based on an interference field of 4600 gr/mm in the SBIL system, corresponding to use of a reference grating with a density of 460 gr/mm on the wafer, and the movement distance and speed of the worktable during this process were set at 12 mm and 1 mm/s, respectively. Through the diffraction light detector in the SBIL system, Fig. 6 presents images of the light spot in the stationary state and the changes in the average intensity within a $0.2 \times 0.2\text{mm}^2$ area during movement of the worktable before and after the dynamic alignment process. The results clearly show that under different deviation angle conditions, the intensity received by the area showed different change periods during the scanning processes of 1.8 mm and 12 mm. As a result, it can be calculated using Eq. (6) that the corresponding deviation angle of the sample shown in Fig.6 was reduced from 0.007° to 0.001°. Therefore, using the dynamic alignment process, ultra-high alignment accuracy between the reference grating and the interference fringes can be achieved, and the composite error of the entire alignment process described in Section 2. can be calculated to be 0.038°. Because of the independence of the errors from each step during alignment process, it is clear that the composite error is mainly contributed by the alignment error that occurs between the reference grating and the spoke in the <111> orientation, and this error can easily be optimized further by optimizing the pattern for the fan-shape spokes and the slit on the contact mask. For example, for a reference grating fabrication error of within 0.01° [14], the total alignment process error would be reduced to 0.018°, which represents better accuracy than the conventional methods.

3. Results and discussion

3.1. Fabrication of 500 gr/mm HARSG

Deep etching of the 500 gr/mm silicon grating was firstly conducted to verify the reliability of the reference grating alignment method described in Section 2.1. The grating pattern was aligned with the <111> crystal orientation and exposed to the photoresist (BP212, Kempur Microelectronics) through a UV contact lithography system, and was then transferred into the 40-nm-thick silicon nitride layer through the ICP etching method by using the pattern as a wet-etching mask. The wafer was etched in a 50 wt% KOH solution with 0.5 wt% of 2,4,7,9-tetramethyl-5-decyne-4,7-diol (TMDD) surfactant for 72 h at approximately 25°C. A critical point dryer (K850, Quorum Technologies) was eventually used after removal of the wafer from the solution to prevent adhesion of the grating lines due to uneven surface tension [13]. Fig. 7 (b) shows the etching results for a 500 gr/mm HARSG with depth of 95.9 μm, 0.47 μm line width, and an undercut of 0.31 μm; these results correspond to an aspect ratio of 204 and an etch rate ratio of 309, which are unusually high when compared with previous reports. The ultra-high etch rate ratio between the vertical direction and the side wall indicated that the grating lines direction was oriented precisely parallel to the (111) plane, and similar experiments have demonstrated good repeatability even for shorter fan-mask spokes; this showed that the alignment between the reference grating and the <111> orientation was sufficiently precise to enable fabrication of the HARSG.

3.2. Fabrication of high groove density deep etching silicon grating

Higher groove density silicon gratings with ultra-high aspect ratio were fabricated using the alignment method described in Section 2 based on the scanning interference field exposure system. A 450 gr/mm grating was first fabricated on the wafer to act as the reference grating; thereafter, interference fields with groove densities of 1800 gr/mm and 3600 gr/mm were aligned with the reference grating before subsequent exposure on the photoresist layer (S1805, Dow). The photoresist mask pattern was then transferred into the silicon nitride layer via ICP etching. Unlike the process in Section 3.1, a chromium supporting mesh mask with a thickness of 100 nm was subsequently fabricated on the silicon nitride layer using a standard lift-off process to

Optics EXPRESS

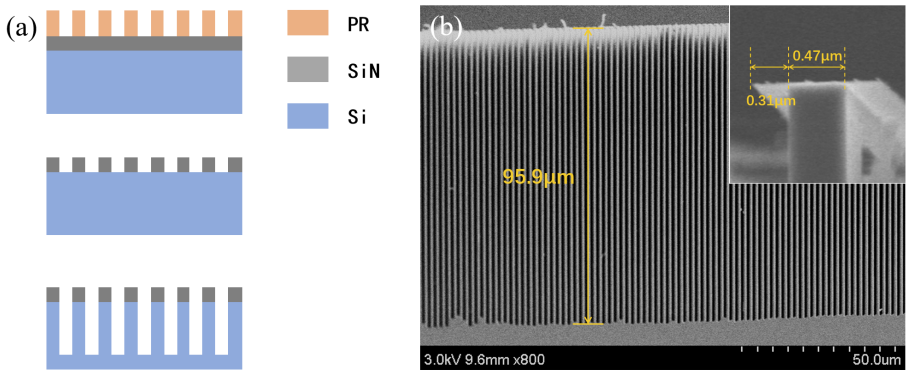

Fig. 7. (a) Schematic diagram of fabrication of the 500 gr/mm HARSG, and (b) SEM sectional view.

improve the stability of the grating structure, as illustrated in Fig. 8. Therefore, the mask that was prepared for wet etching was a combination of both the silicon nitride grating mask and the chromium supporting mesh mask. The wafer was eventually etched in a 50 wt% KOH solution containing 0.5 wt% of TMDD surfactant. Fig. 9 shows the results of etching of the 1800 gr/mm grating mask in a 19-20°C etch solution for 20 h, indicating an etch depth of 16.8 μm and a line width of 0.15 μm, which corresponds to an aspect ratio of 112. Note here that although the SBIL system can produce a large area grating mask to cover the entire wafer, the sizes of the HARSGs fabricated in our experiments were limited by the internal dimensions of the critical point dryer. Similar results are shown in Fig. 10 for another two 1800 gr/mm samples after 10 hours of etching, which presented an etch rate ratio of approximately 210. These results also indicated that the TMDD surfactant did not have a significant effect on the etch rate ratio, and that the slight differences in etch depth between the two samples might be caused by changes in room temperature and differences in the duty cycles of the grating masks. A HARSG with density of 3600 gr/mm was also fabricated by etching for 5 h in a KOH solution, which is shown in Fig. 11 to have a 5.5 μm etch depth and 60 nm line width. It can be concluded from the results presented above that the alignment method based on the SBIL system proposed in our paper can achieve

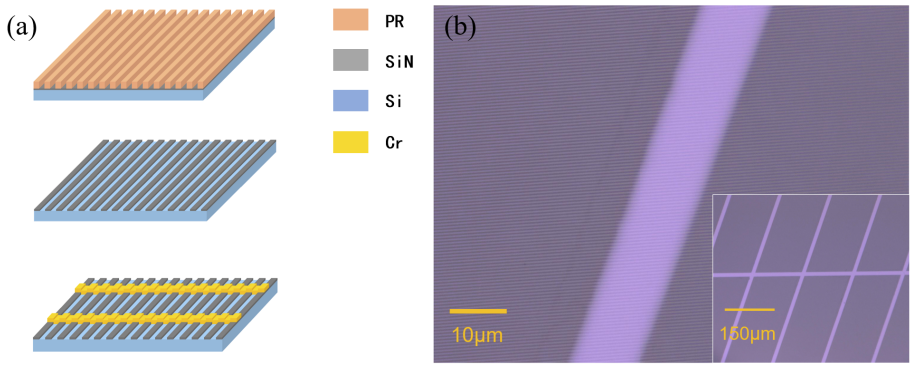

Fig. 8. (a) Schematic diagram of high-groove-density grating mask fabrication process, and (b) microscopic image of the 1800 gr/mm grating mask with a Cr mesh mask. The width of the chrome line is 10 μm, and the length and width of the individual grids are 600 μm and 150 μm, respectively, with an angle of 70.53° corresponding to the angle between the two <111> crystal directions on the (110) plane.

Optics EXPRESS

precise alignment between the holographic grating lines and the <111> crystal orientation, and further obtain excellent anisotropy in the wet etching process.

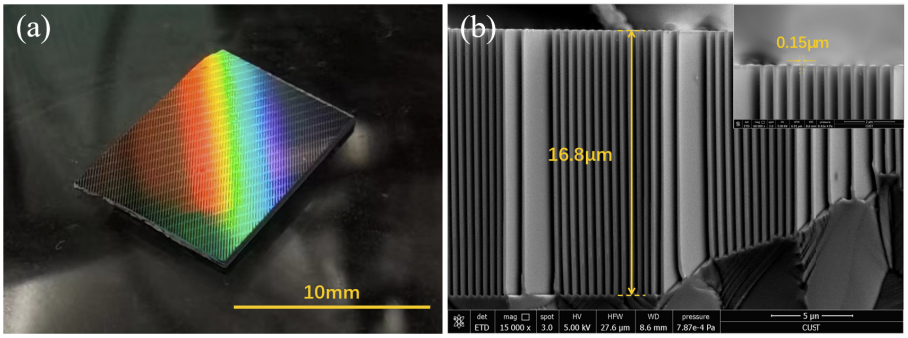

Fig. 9. (a) Image of the 1800 gr/mm HARSG, and (b) SEM sectional view with a declination angle. The inclined plane shown at the bottom of the grating on the right resulted from broadening caused by the supporting mesh mask during the wet etching process.

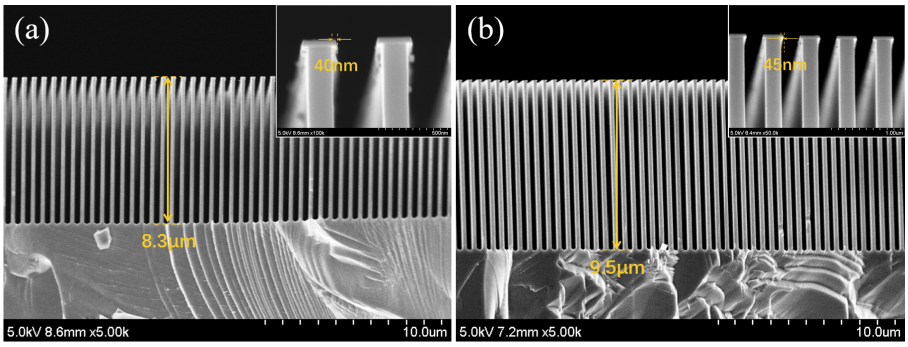

Fig. 10. SEM images of 1800 gr/mm HARSGs when etched for 10 h in (a) a 50 wt% KOH solution with 0.5 wt% TMDD and (b) a KOH solution without the surfactant.

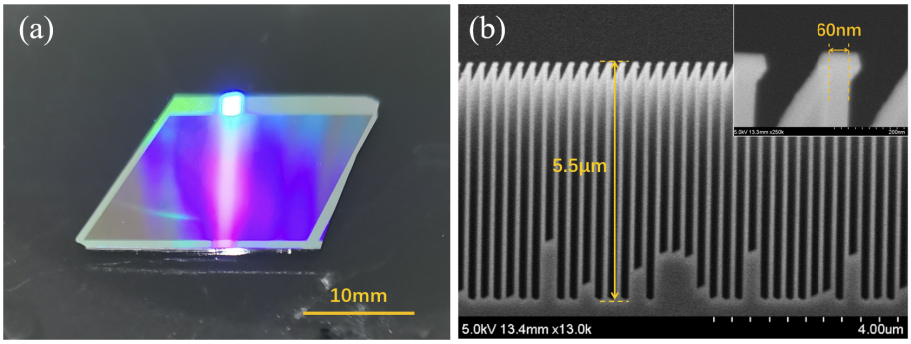

Fig. 11. (a) Image of the 3600 gr/mm HARSG and (b) the SEM sectional view. The mesh mask for the 3600 gr/mm HARSG had a width of 50 μm and length of 200 μm for each grid.

Optics EXPRESS

4. Conclusion

A new method for alignment between the grating lines and the <111> orientation of a silicon wafer based on the SBIL system is proposed in the paper for use in the fabrication of HARSGs. Through interference of the diffracted light beams from the reference grating, a composite error of 0.038° can be achieved when using the proposed alignment method, and each process step has been verified via anisotropic wet etching experiments, which showed good stability and eventually obtained HARSGs with groove densities of 500 gr/mm, 1800 gr/mm, and 3600 gr/mm with ultra-high aspect ratios and etch rate ratios. Compared with the alignment methods that were used in previous studies, the method in our paper provides both convenience and high precision, and offers good compatibility for the SBIL system without the need to introduce additional components into the system. Furthermore, the accuracy of the method can easily be improved further by changing the contact mask pattern presented in Section 2.1. It should also be noted that the alignment method can be applied to the static holographic interference lithography system without a requirement for drastic changes, which can improve the alignment accuracy of the static holographic exposure system greatly for requiring fewer intermediate steps when compared with the previous method.

Funding. National Key Research and Development Program of China (2020YFA0714500); Key core technology research project of the Chinese Academy of Sciences (E00832GZH1); Jilin Province Science & Technology Development Program in China (20200602051ZP); Natural Science Foundation of Jilin Province (20210101139JC); National Natural Science Foundation of China (61905244).

Acknowledgments. This work is supported by National Key Research and Development Program of China (2020YFA0714500); Key core technology research project of the Chinese Academy of Sciences(E00832GZH1); Jilin Province Science & Technology Development Program in China(20200602051ZP); Natural Science Foundation of Jilin Province(20210101139JC); National Natural Science Foundation of China(61905244).

Disclosures. The authors declare no conflicts of interest.

Data availability. Data underlying the results presented in this paper are not publicly available at this time but may be obtained from the authors upon reasonable request.

References

1. V. Egorov, M. Eitan, and J. Scheuer, "Genetically optimized all-dielectric metasurfaces," Opt. Express **25**(3), 2583–2593 (2017).
2. L. Ye, G. Zhang, and Z. You, "Large-aperture khz operating frequency ti-alloy based optical micro scanning mirror for lidar application," Micromachines **8**(4), 120 (2017).
3. P. Levin, E. Ashkenazy, A. Raz, M. Hershcovitz, S. Bouwstra, D. Mendlovic, and S. Krylov, "A wafer level packaged fully integrated tunable fabry-pérot filter with extended optical range for multispectral and hyperspectral imaging," J. Microelectromech. Syst. **29**(3), 357–369 (2020).
4. T. Weitkamp, A. Diaz, C. David, F. Pfeiffer, M. Stampanoni, P. Cloetens, and E. Ziegler, "X-ray phase imaging with a grating interferometer," Opt. Express **13**(16), 6296–6304 (2005).
5. Y. Du, X. Liu, Y. Lei, J. Guo, and H. Niu, "Non-absorption grating approach for x-ray phase contrast imaging," Opt. Express **19**(23), 22669–22674 (2011).
6. F. G. Meinel, F. Schwab, A. Yaroshenko, A. Velroyen, M. Bech, K. Hellbach, J. Fuchs, T. Stiewe, A. Ö. Yildirim, F. Bamberg, M. F. Reiser, F. Pfeiffer, and K. Nikolaou, "Lung tumors on multimodal radiographs derived from grating-based x-ray imaging–a feasibility study," Physica Medica **30**(3), 352–357 (2014).
7. P. S. Finnegan, A. E. Hollowell, C. L. Arrington, and A. L. Dagel, "High aspect ratio anisotropic silicon etching for x-ray phase contrast imaging grating fabrication," Mater. Sci. Semicond. Process. **92**, 80–85 (2019).
8. L. Romano, J. Vila-Comamala, K. Jefimovs, and M. Stampanoni, "High-aspect-ratio grating microfabrication by platinum-assisted chemical etching and gold electroplating," Adv. Eng. Mater. **22**(10), 2000258 (2020).
9. R. K. Heilmann, A. R. Bruccoleri, and M. L. Schattenburg, "High-efficiency blazed transmission gratings for high-resolution soft x-ray spectroscopy," in *Optics for EUV, X-Ray, and Gamma-Ray Astronomy VII*, vol. 9603 (SPIE, 2015), pp. 296–307.
10. H. Günther and R. K. Heilmann, "Lynx soft x-ray critical-angle transmission grating spectrometer," Journal of Astronomical Telescopes, Instruments, and Systems **5**, 021003 (2019).
11. R. K. Heilmann, A. R. Bruccoleri, and J. Song, "Manufacture and performance of blazed soft x-ray transmission gratings for arcus and lynx," in *Optics for EUV, X-Ray, and Gamma-Ray Astronomy X*, vol. 11822 (SPIE, 2021), pp. 206–216.
12. H. Seidel, L. Csepregi, A. Heuberger, and H. Baumgärtel, "Anisotropic etching of crystalline silicon in alkaline solutions: Ii. influence of dopants," J. Electrochem. Soc. **137**(11), 3626–3632 (1990).

Optics EXPRESS

13. M. Ahn, R. K. Heilmann, and M. L. Schattenburg, "Fabrication of 200nm period blazed transmission gratings on silicon-on-insulator wafers," J. Vac. Sci. Technol. B **26**(6), 2179–2182 (2008).
14. Y. Zheng, K. Qiu, H. Chen, Y. Chen, Z. Liu, Y. Liu, X. Xu, and Y. Hong, "Alignment method combining interference lithography with anisotropic wet etch technique for fabrication of high aspect ratio silicon gratings," Opt. Express **22**(19), 23592–23604 (2014).
15. Y. Wang, S. Li, T. Wu, F. Hu, and Z. Cao, "Fabrication of freestanding nanoscale gratings on silicon-on-insulator wafer," Appl. Phys. A **117**(4), 2101–2105 (2014).
16. A. R. Bruccoleri, "Fabrication of high-throughput critical-angle x-ray transmission gratings for wavelength-dispersive spectroscopy," Ph.D. thesis, Massachusetts Institute of Technology (2013).
17. L. Romano, J. Vila-Comamala, M. Kagias, K. Vogelsang, H. Schift, M. Stampanoni, and K. Jefimovs, "High aspect ratio metal microcasting by hot embossing for x-ray optics fabrication," Microelectron. Eng. **176**, 6–10 (2017).
18. K. Li, M. J. Wojcik, R. Divan, L. E. Ocola, B. Shi, D. Rosenmann, and C. Jacobsen, "Fabrication of hard x-ray zone plates with high aspect ratio using metal-assisted chemical etching," Journal of Vacuum Science & Technology B, Nanotechnology and Microelectronics: Materials, Processing, Measurement, and Phenomena **35**, 06G901 (2017).
19. L. Romano, M. Kagias, J. Vila-Comamala, K. Jefimovs, L.-T. Tseng, V. A. Guzenko, and M. Stampanoni, "Metal assisted chemical etching of silicon in the gas phase: A nanofabrication platform for x-ray optics," Nanoscale Horiz. **5**(5), 869–879 (2020).
20. Y. Zheng, C. Li, H. Hu, S. Huang, Z. Liu, and H. Wang, "Metal-assisted chemical etching of high throughput, high aspect ratio critical-angle transmission gratings with vertical and smooth sidewalls," Jpn. J. Appl. Phys. **60**(3), 035003 (2021).
21. M. Ahn, "Fabrication of critical-angle transmission gratings for high efficiency x-ray spectroscopy," Ph.D. thesis, Massachusetts Institute of Technology (2009).
22. Y. Song, W. Wang, S. Jiang, Bayanheshig, and N. Zhang, "Weighted iterative algorithm for beam alignment in scanning beam interference lithography," Appl. Opt. **56**(31), 8669–8675 (2017).
23. S. Jiang, B. Lü, Y. Song, Z. Liu, W. Wang, L. Shuo, and Bayanheshig, "Heterodyne period measurement in a scanning beam interference lithography system," Appl. Opt. **59**(19), 5830–5836 (2020).
24. Z. Liu, H. Yang, Y. Li, S. Jiang, W. Wang, Y. Song, W. Li, and Bayanheshig, "Active control technology of a diffraction grating wavefront by scanning beam interference lithography," Opt. Express **29**(23), 37066–37074 (2021).